Green Chemistry

PAPER

View Article Online
View Journal | View Issue

Cite this: *Green Chem.*, 2026, **28**, 4947

One pot synthesis of L-xylose from formaldehyde with an improved benzoylformate decarboxylase

Junhui Zhou,[a] Florian Bourdeaux, [a] Tianwei Tan*[b,c,e] and Ulrich Schwaneberg *[a,d]

Formaldehyde (FALD), which can be derived from CO_2, is a promising C1 feedstock for enzymatic synthesis of valuable chemicals, like sugars, starch, acetyl-CoA, and lactic acid. Rare sugars, like L-xylose, have great potential for pharmaceutical applications, but their production requires precise control of stereocenters, a challenge that can be addressed by enzymatic catalysis. To date, no enzymatic route to produce L-xylose from only FALD has been reported. In this report, thermal resistance of a highly active and specific glycolaldehyde (GALD) producing benzoylformate decarboxylase variant from *Polynucleobacter necessarius* (PnBFD-M1) was improved *via* rational design, yielding PnBFD-M2 (PnBFD-M1-K188I/Q192I/A282P). PnBFD-M2 exhibits improved thermal resistance (T_m +11.2 °C; $t_{1/2}$ at 37 °C increased from 44 min to 2247 min) and moderately enhanced initial GALD production rate (from 302.9 μmol per (min g protein) to 350.3 μmol per (min g protein)). Analysis of the surface hydrophilicity and molecular dynamics simulations indicate that the improved thermal resistance is based on hydrophobic substitutions that stabilize the contact of two helices and increased rigidity. The small increase of activity seems to be caused by the reduced flexibility of loops located near the active site. The engineered PnBFD-M2 was successfully coupled with a fructose-6-phosphate aldolase variant (FSA-A129T/A165G) to achieve the first one-pot enzymatic synthesis of L-xylose from FALD as sole feedstock, reaching a titer of 2.36 g L^{-1} and a yield of 78% (outperforming PnBFD-M1: 1.76 g L^{-1} and 59%). PnBFD-M2 is one of the most efficient GALD from FALD producing enzymes known to date: almost no side products are formed (<1% 1,3-dihydroxyacetone is produced) and PnBFD-M2 has higher thermal resistance and higher activity compared to GALS-F397Y/C398M ($t_{1/2}$ at 37 °C is <120 min). The presented L-xylose pathway is an interesting biocatalytic route to produce L-xylose directly from FALD showing the potential of C1 valorization.

Received 4th December 2025,
Accepted 12th February 2026

DOI: 10.1039/d5gc06542a

rsc.li/greenchem

Green foundation

1. This work establishes the first biocatalytic route for synthesizing L-xylose using formaldehyde as the sole feedstock, a C1 substrate obtainable from CO_2.
2. The engineered ThDP-dependent enzyme PnBFD-M2 exhibits high catalytic efficiency and markedly enhanced thermal stability, enabling robust conversion of formaldehyde to glycolaldehyde with minimal side-product formation (<1%).
3. PnBFD-M2 is a robust and efficient biocatalyst well suited for cascades and metabolic pathways involving formaldehyde condensation, advancing CO_2 valorization toward value-added chemicals.

Introduction

With CO_2 being one of the major contributors to climate change, there is a strong need to turn this current waste product into a feedstock for various industries.[1] In recent years, biotechnological methods such as metabolic engineering,[2] synthetic biology,[3] and enzyme catalysis[4] have been employed to produce synthetical important compounds from CO_2 or C1 molecules, including methanol, formic acid and formaldehyde (FALD), which can be obtained from the reduction of CO_2.[5–9] FALD serves as a key building block in the production of everyday commodities, including biocides, disinfectants, preservatives, adhesives, and resins.[6] Global FALD production is estimated to exceed 45.6 million metric tons per year, with demand continuing to grow steadily.[6] The majority of FALD is currently produced by catalytic oxidation of metha-

[a]*Institute for Biotechnology RWTH Aachen University, Worringer Weg 3, 52074 Aachen, Germany. E-mail: u.schwaneberg@biotec.rwth-aachen.de*
[b]*Beijing Key Lab of Bioprocess, National Energy R&D Center for Biorefinery, Beijing 100029, PR China. E-mail: twtan@mail.buct.edu.cn*
[c]*College of Life Science and Technology, Beijing University of Chemical Technology, Beijing 100029, PR China*
[d]*Beijing University of Chemical Technology, Beijing 100029, PR China*
[e]*State Key Laboratory of Green Biomanufacturing, Beijing 100029, PR China*

nol *via* the FORMOX process, employing iron-molybdenum oxide catalysts at 300–400 °C, or *via* related silver-catalyzed processes.[10] Industrial FALD production is therefore tightly coupled to methanol supply, which is still dominated by fossil feedstocks, primarily natural gas and coal, whereas renewable methanol accounts for only about 0.2% of global production.[11] Although the direct production of methanol and FALD from CO_2 has been demonstrated and is widely regarded as a promising route toward defossilization, these technologies require further development before they can compete with established industrial processes.[11,12] In the context of ongoing technological development, hybrid approaches that combine electrochemical CO_2 reduction with enzymatic transformation of the resulting C1 intermediates may represent a promising strategy for the sustainable synthesis of high-value compounds. Such concepts aim to exploit the superior reaction kinetics and scalability of electrochemical CO_2 reduction,[1] while simultaneously benefiting from the high selectivity, mild operating conditions, and environmentally benign nature of enzymatic catalysis.[13]

By utilizing multi-enzyme cascades, products like starch,[14] acetyl-CoA,[15] glucose,[16] polyhydroxybutyrate (PHB),[17] ethylene glycol,[18,19] glycolic acid,[19,20] erythrose,[19] erythrulose,[21] alanine,[22] hexoses,[23] lactic acid,[24,25] xylulose,[26] and L-threitol[27] were produced from C1. For the enzymatic synthesis of high-value chemicals, like rare sugars, which find usage in the pharma industry, FALD with its higher reactivity compared to other C1 compounds,[28] such as formic acid and methanol, is an ideal carbon source for multi enzyme cascades. Most of these cascades utilize enzymes that condense two FALD molecules to glycolaldehyde (GALD), that then is further transformed, stepwise increasing the complexity of the product,[15,17] for example, the rare sugar L-xylose can be produced by the enzyme D-fructose-6-phosphate aldolase (FSA), specifically the variant FSA-A129T/A165G (FSA-TG), utilizing FALD and GALD as the substrates.[29]

L-Xylose is a rare pentose sugar and an attractive starting material for the synthesis of pharmaceutically active molecules and functional sugars, with increasing relevance in pharmaceutical and nutraceutical applications.[30–32] Its nucleoside analogues are utilized as antiviral drugs against hepatitis-B and HIV, along with valuable anticancer and cardioprotective properties.[33,34] Recently developed L-xylose derivatives have shown potential as inhibitors of renal glucose reabsorption, making them attractive candidates for diabetes treatment.[35] Furthermore, polyhydroxypyrrolidines derived from L-xylose demonstrate both antitumor and antiviral effects and act as potent inhibitors of α- and β-glucosidases, which are key targets in the development of antidiabetic drugs.[36] With the continuous expansion of the antiviral and metabolic disorder drug markets, L-xylose derivatives are expected to commercial value.[37] Reported syntheses of L-xylose from xylitol (one step, 26% product specificity),[36] D-glucose (four steps, involving hazardous reagents such as Ag_2CO_3, and periodic acid),[38] D-gluconolactone (four steps, involving environmentally unfriendly conditions such as *N*,*N*-dimethylformamide (DMF) and BCl_3),[35] and L-xylulose (one step, 85% product specificity)[31] are generally characterized by low selectivity, multiple reaction steps, or the use of hazardous reagents and solvents. A notable exception is the L-xylulose-based route, which achieves comparatively high product specificity (85%).

In this context, enzymatic pathways capable of condensing FALD into GALD and subsequently converting it into higher sugars represent a potentially attractive alternative. However, despite their academic appeal, the economic and environmental viability of synthesizing L-xylose from FALD remains difficult to assess at present. In the absence of a detailed techno-economic assessment (TEA), it is not yet clear whether an enzymatic route (requiring both enzyme production and a sustainable supply of FALD) would ultimately outperform established chemical or biomass-derived processes in terms of overall sustainability.

Several GALD-producing enzymes that utilize FALD have been identified, such as benzaldehyde lyases (BAL),[39] benzoylformate decarboxylases (BFD),[15] and glyoxylate carboligases (GCL).[18] All these enzymes dependent on thiamine pyrophosphate (TPP) as cofactor and can stepwise condensate FALD molecules to larger molecules, like two FALD molecules are condensed to GALD, which can then react with a third FALD to produce 1,3-dihydroxyacetone (DHA) or undergo condensation with another GALD to synthesize erythrulose.[18,39,40] FALD is not the natural substrate for any of the these enzymes, and the wild-type enzymes have been reported to exhibit low FALD condensation activity (<10 U g^{-1}).[41] Multiple engineering campaigns were conducted to enhance their activity, resulting in several improved enzymes, including FLS,[14,39] which mainly synthesizes DHA, as well as GALS[15] and GCL[18] variants that primarily produce GALD. To date, the most active GALD-producing enzymes are GALS-F397Y/C398M (GALS-YM)[17] and the BFD variant from *Polynucleobacter necessarius* PnBFD-M1.[41] GALS-YM has higher thermal resistance compared to PnBFD-M1 (T_m(GALS-YM) = 50.8 °C, T_m(PnBFD-M1) = 38 °C) but produces high amounts of DHA (21.01%), while PnBFD-M1 produces mainly GALD (99.5%).[41] The production of unwanted side products is for *in vitro* and *in vivo* cascades problematic as it lowers overall yields and the side products might inhibit other steps/reactions.[42]

Improving both thermal resistance and activity of GALD-producing enzymes through protein engineering is challenging, as these properties are often inversely related: flexibility generally enhances activity, whereas rigidity favors thermal stability.[43–46] Thermal resistance of enzymes was successfully improved by rational design and directed evolution,[47–49] but as a general trend, specific activity is often reduced.[50] For instance, the T_m of *Candida* ketoreductase variant M1 increased by 4 °C, whereas its activity decreased to 88% of that of the wild-type enzyme.[51] A general design principle to improve the thermal resistance of enzymes is to increase the rigidity of flexible regions.[52,53] Flexible regions can be identified based on *B*-factor analysis, if a crystal structures with a high resolution is available,[48] or based on computational methods.[54,55] The introduction of proline residues into flexible loops was reported to be an effective strategy

to enhance thermal resistance.[56–58] Remarkable results were also reported by analyzing thermodynamic stability (free energy of folding $\Delta\Delta G$) using computational tools such as FoldX, Rosetta, I-mutant, Mupro, DeepDDG or PremPS.[59–63] In detail, both approaches have shown promising results in the engineering of lipases[64,65] and PETases.[66–68] Rare simultaneous improvements in both enzymatic activity and thermal resistance can be found in literature, for example the engineering of α-galactosidase,[46] ulvan lyase,[69] and aldehyde dehydrogenase.[43]

In this report, PnBFD-M1 was improved through rational design approaches, resulting in a thermal resistance increase (T_m increased by 11 °C; $t_{1/2}$ at 37 °C increased from 44 min to 2247 min) and an enhancement in activity (initial GALD production rate increased from 302.9 μmol per (min g protein) to 350.3 μmol per (min g protein)). MD simulations indicate that the improved specific activity and thermal resistance can be attributed to decreased flexibility of β domain. The improved PnBFD variant, PnBFD-M2 (PnBFD-M1-K188I/Q192I/A282P), is to our knowledge the most efficient GALD producing enzyme (<1% DHA is produced) while having a higher stability than GALS-YM ($t_{1/2}$ at 37 °C is <120 min). To show the potential of PnBFD-M2, it was used with FSA-TG to produce L-xylose directly from FALD in a one pot reaction, achieving a titer of up to 2.36 g L^{-1}, corresponding to 78% of the theoretical yield.

Results and discussion

The production of L-xylose from FALD requires PnBFD variants that efficient produce GALD without the side product; GALD is subsequently converted to glyceraldehyde (GCA) and then to L-xylose by the enzyme FSA-TG. PnBFD-M1 is an attractive enzyme since it can produce GALD (99.5% GALD, without producing high amounts of side product DHA), but its low thermal resistance limits L-xylose production (T_m = 38 °C).[41] Therefore, for the construction of an efficient L-xylose producing cascade, the thermal resistance of PnBFD-M1 was enhanced through a rational design strategy based on $\Delta\Delta G$ calculations and proline substitutions in flexible loops. The most promising PnBFD-M1 variants were characterized and molecular dynamics (MD) simulations were conducted to uncover the structural basis for improved enzyme performance. The new variant PnBFD-M2 (T_m = 49.2 °C) was then used in a first one pot cascade under optimized conditions to maximize the L-xylose titer.

Design of L-xylose pathway from C1

Efficient chemical reduction of CO_2 to FALD has been reported,[5] making FALD a feasible and attractive C1 building block for the synthesis of various valuable compounds.[6] L-Xylose is a precursor for pharmaceutically interesting molecules,[31] but current syntheses require multiple steps with an overall low product specificity (26%).[31,36] It was reported that L-Xylose can be produced from FALD and GALD by the FSA-TG.[29] FSA-TG catalyzes the aldol condensation of FALD and GALD to form GCA, that is then transformed in a second aldol reaction with GALD to L-xylose.[29] Therefore, by combining a GALD producing enzyme, like PnBFD-M1, with the enzyme FAS-TG a L-xylose producing cascade that only requires FALD as feedstock can be built (Fig. 1A). In our previous study, PnBFD-M1 demonstrated high specificity (99.5% GALD) for the conversion of FALD to GALD but suffers from low thermal resistance, losing 80% of its activity after incubation at 37 °C for 1 h.[41] The low thermal resistance limits the use of PnBFD for the production of GALD and the its application in enzyme cascade, for example for the production of L-xylose, since FSA-TG displays a higher thermal resistance (T_m = 74 °C), which would allow higher process temperatures. Therefore, a more thermal resistant variant of PnBFD was designed *via* two rational design strategies and tested in a one-pot reaction.

Improving PnBFD-M1 *via* rational design

PnBFD-M1 belongs to the TPP-dependent enzyme family and adopts a homo-tetrameric structure (Fig. S1A), which can be further divided in to two dimers having the active sites located at this dimeric interface. Each monomer consists of three domains. In most of BFDs, the α domain (Residues 1–178 of PnBFD-M1) and the γ domain (Residues 339–535 of PnBFD-M1) build up the catalytic site, while the β domain (Residues 179–338 of PnBFD-M1) has a structural role by stabilizing the two other domains[70–72] (Fig. S1B). The deletion of the β domain of PnBFD-M1 resulted in no soluble protein, highlighting its critical role in maintaining structural integrity (Data not show). To enhance thermal resistance of PnBFD-M1 without compromising the overall activity or as little as possible, two rational design strategies were applied to the β domain: (1) virtual screening of potential variants based on predicted changes in Gibbs free energy ($\Delta\Delta G$ value) calculated using FoldX, DeepDDG, and I-Mutant (based on the method reported by the Yuguo Zheng group[60]), and (2) increasing the rigidity of flexible loops by introducing prolines (Fig. 1B). In strategy (1), potential positions for amino acids exchanges were identified by calculating the root mean square fluctuations (RMSF) of each position of the β-domain of PnBFD-M1 at 310 K based on MD simulations. Residues with an RMSF ≥ 2 Å were selected and $\Delta\Delta G$ values for each amino acid exchange calculated using FoldX, DeepDDG, and I-Mutant 2.0. Variants that met the set cut off in the predicted increase in stability (FoldX: $\Delta\Delta G \leq$ +0,36 kcal mol^{-1}; DeepDDG: $\Delta\Delta G >$ 0 kcal mol^{-1}; I-mutant 2.0: $\Delta\Delta G >$ 0 kcal mol^{-1})[60,73] were selected for experimental validation. In strategy (2), loop/unstructured regions within the β-domain were identified by analyzing the structure of PnBFD (PDB: 4K9Q). Flexible regions were identified by comparing the predicted RMSF values of each residue within long loop regions at 310 K and 340 K, since flexible regions should exhibit greater fluctuations at elevated temperatures.[60] Residues in long loop regions (more than 5 amino acids) with an RMSF difference (RMSFi (340 K)–RMSFi (310 K); i selected position) ≥ 0.5 Å were selected, and proline was introduced at each selected position (one per variant) for experimental validation. After experimental validation the most stable variants of each strategy were combined and the new variant (PnBFD-M2) was charac-

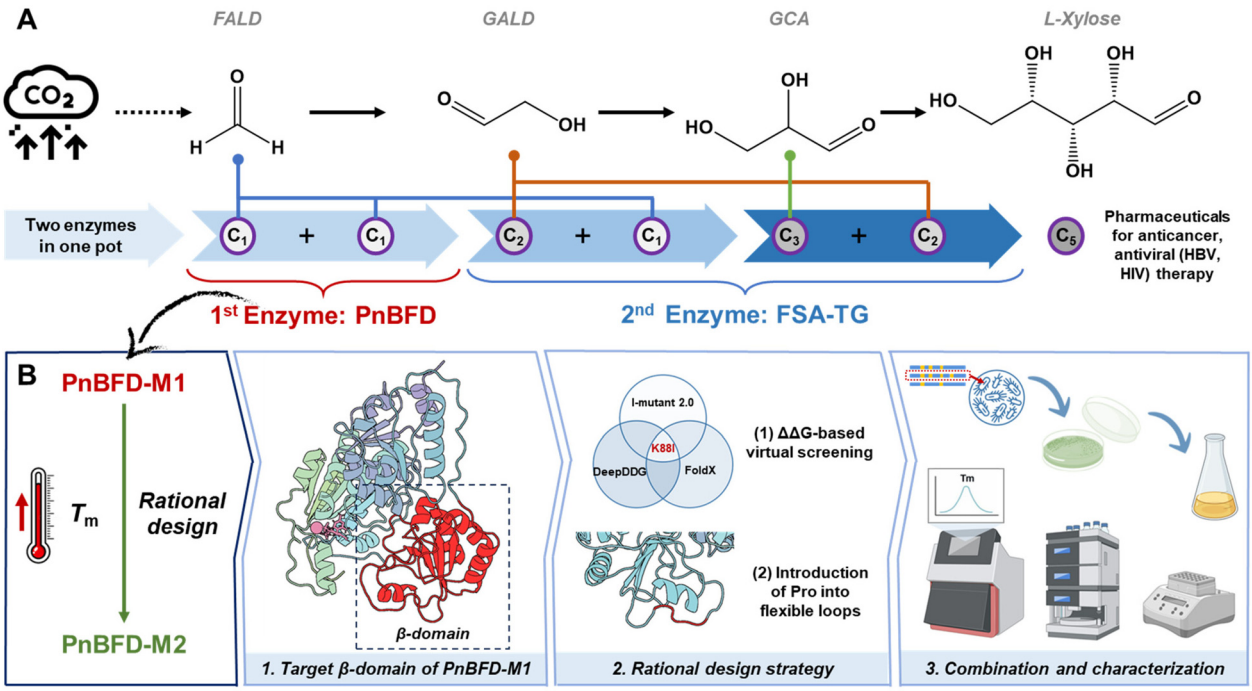

Fig. 1 (A) Design of L-xylose biosynthetic pathway from C1: PnBFD-M1 and FSA-TG cascade with PnBFD-M1 as the thermosensitive bottleneck. (B) Rational design strategy of β-domain of PnBFD-M1 and recombination of beneficial variants, resulting in PnBFD-M2 with improved thermal resistance and catalytic activity.

terized. To test if the improved thermal resistance of PnBFD-M2 is beneficial in enzymatic cascades, it was combined with FSA-TG to produce L-xylose from FALD in a one-pot reaction setup.

As basis for the $\Delta\Delta G$ calculations of strategy 1, three independent 100 ns MD simulations of PnBFD-M1 at 310 K were conducted. The RMSF of the position of each amino acid of the β-domain was calculated using the stable trajectory stage (50–100 ns) based on root mean square deviation (RMSD) of the Cα atoms (Fig. 2; RMSD of Cα atom positions of PnBFD-M1 at 310K was reported in Fig. S13A of our previous report[39]). 12 residues, exhibiting an RMSF ≥ 2 Å at 310 K (Table S3), were selected for virtual site-saturation mutagenesis (SSM) screening using FoldX, DeepDDG, and I-Mutant 2.0. 9 potential variants, which were predicted by all three tools to have the potential to improve thermal resistance (Table 1), were subsequently targeted experimental validation.

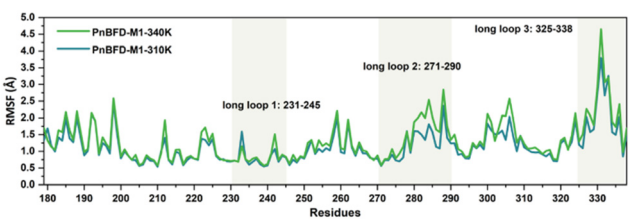

Fig. 2 RMSF (50–100 ns) of the β-domain of PnBFD-M1 at 310 K and 340 K.

Table 1 Potential variants predicted based on $\Delta\Delta G$ calculations

Variants	FoldX (kcal mol^{-1})	DeepDDG (kcal mol^{-1})	I-Mutant2.0 (kcal mol^{-1})
K188I	−0.33	0.01	0.44
Q192I	−0.29	0.04	0.33
K259I	0.02	0.02	0.27
K259M	−0.75	0.11	0.09
D327Q	0.23	0.06	0.46
D327E	0.03	0.11	0.19
K331R	−0.58	0.27	0.30
Q336I	−0.90	0.04	0.43
Q336V	0.13	0.03	0.38

FoldX: $\Delta\Delta G \leq +0{,}36$ kcal mol^{-1}; DeepDDG: $\Delta\Delta G > 0$ kcal mol^{-1}; I-mutant 2.0: $\Delta\Delta G > 0$ kcal mol^{-1}.

Each variant was produced in *Escherichia coli* (*E. coli*), purified and the activity (measured as GALD production using HPLC) and stability were determined. 6 of the 9 variants (K188I, Q192I, D327E, K331R, Q336I and Q336 V) exhibit either unchanged or increased activity, with Q192I enhancing the relative activity by 2.47 times (Fig. 3A). The T_m of these 6 variants was determined with the Prometheus NT.48 (Nanotemper) by measuring the tryptophan fluorescence at increasing temperatures. Measurements with PnBFD-M1 revealed two melting events (T_{m1} = 38.0 °C, T_{m2} = 43.9 °C), likely due to its multi domain structure (Fig. S2A and Table 2). Another explanation could be that one of the melting events is caused by the dissociation of the homotetramer (Fig. S1A) and

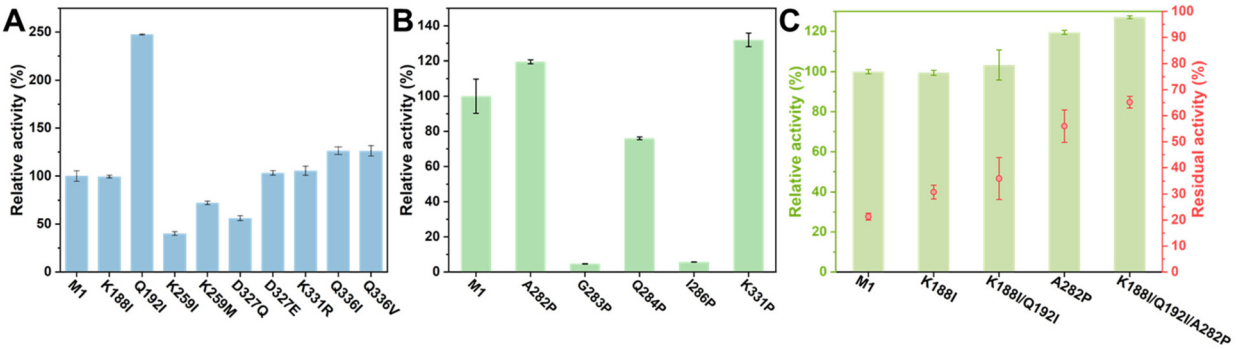

Fig. 3 (A) Relative activity of PnBFD-M1 and 9 potential variants of ΔΔ*G* calculations strategy. (B) Relative activity of PnBFD-M1 and 5 potential variants of introducing Pro in long loops strategy. (C) Relative activity of PnBFD-M1, M1-K188I, M1-K188I/Q192I, and PnBFD-M2 (M1-K188I/Q192I/A282P), and their residual activity after heat treatment at 40 °C for 30 min. Relative activity assay: 50 mM pH 7.6 bicine, 300 mM NaCl, 1 mM TPP, 2 mM $MgSO_4$, 0.2 mg mL^{-1} purified enzyme, and 10 mM FALD, the reaction mixture was incubated at 37 °C for 30 min. Residual activity assay: 50 mM pH 7.6 bicine, 300 mM NaCl, 1 mM TPP, 2 mM $MgSO_4$, 0.2 mg mL^{-1} enzyme after heat treatment at 40 °C for 30 min, and 10 mM FALD, the reaction mixture was incubated at 37 °C for 30 min; Error bars represent standard deviation of three technical replicates (n = 3).

Table 2 T_m values of PnBFD-M1 and its variants

Variants	T_{m1} (°C)	T_{m2} (°C)
PnBFD-M1	38.0 ± 0.0	43.9 ± 0.0
K188I	43.7 ± 0.1	
Q192I	39.1 ± 0.1	44.4 ± 0.0
D327E	44.0 ± 0.1	
K331R	38.0 ± 0.0	44.1 ± 0.1
Q336I	38.0 ± 0.0	43.5 ± 0.0
Q336V	38.0 ± 0.0	43.2 ± 0.1
K188I/Q192I	44.4 ± 0.1	
A282P	43.6 ± 0.1	48.3 ± 0.1
K331P	38.3 ± 0.1	43.6 ± 0.0
K188I/Q192I/A282P (PnBFD-M2)	49.2 ± 0.1	

thereby induced structural changes. The variant K188I showed the highest increase in T_m (6 °C) and displayed only one peak. The variant Q192I still displayed two melting points, but both T_{m1} and T_{m2} are slightly higher than those of PnBFD-M1. Like the variant K188I, also the variant D327E displayed only one distinct unfolding event, but in contrast to variant K188I a shoulder at about 35 °C to 39 °C was visible. Both residues K188 and Q192 are solvent exposed and located on the same α helix in the β domain. The closest side chain to these two residues is the side chain of L325, an exchange to more hydrophobic residues therefore should be beneficial, by strengthening the hydrophobic interactions.

Based on these results a variant combining K188I and Q192I (M1-K188I/Q192I) was produced and characterized M1-K188I/Q192I has a slightly higher activity than PnBFD-M1 and M1-K188I, and its residual activity after 30 min incubation at 40 °C is higher than that of PnBFD-M1 and slightly higher than that of M1-K188I (Fig. 3C). M1-K188I/Q192I has also a higher T_m compared to M1-K188I and PnBFD-M1 and showed similar to M1-K188I only a single melting event, showing that both mutations act synergistic (Fig. S2A and Table 2).

To realize strategy 2 three additional 100 ns MD simulations at 340 K were performed. As described above, the RMSF values of the β-domain during the stable period (50–100 ns) were calculated for the simulation at 340 K and compared with those at 310 K. Since only long unstructured regions should be targeted, to avoid disruption of existing structures in PnBFD by the introductions of prolines, therefore comparison was limited to the regions 231–245, 271–290 and 325–338. 5 residues in the chosen regions have an RMSF difference (RMSFi (340 K)–RMSFi (310 K); i selected position) ≥ 0.5 Å and were selected (Fig. 2, RMSD of the Cα atoms was seen in Fig. S3A). Proline substitutions were introduced at these positions (A282P, G283P, Q284P, I286P and K331P) to enhance rigidity and experimentally characterized. Activity assays showed that only A282P and K331P have higher activity compared to PnBFD-M1 (Fig. 3B). The thermal shift experiments with variant A282P showed similar to PnBFD-M1 two distinct melting events, interestingly T_{m1} is similar to the T_{m1} of PnBFD-M1 but T_{m2} is 4 °C higher than the T_{m2} of PnBFD-M1 (Fig. S2B and Table 2). The variant K331P showed similar thermal resistance as PnBFD-M1.

Since M1-K188I/Q192I has only one melting point, assuming this one is corresponding to T_{m2}, and M1-A282P increases T_{m2} there should be synergistic effects then combining these variants. As expected, M1-K188I/Q192I/A282P (PnBFD-M2) showed only one melting event in the melting curve with a melting point of 49.2 °C, which is 11.2 °C and 5.3 °C higher than T_{m1} and T_{m2} of PnBFD-M1, respectively (Fig. S2B and Table 2). Further activity measurements revealed a 1.27-fold improvement in relative activity compared to PnBFD-M1 (Fig. 3C). The residual activity of PnBFD-M2 after incubating at 40 °C for 30 min is 65%, approximately three times that of PnBFD-M1.

Characterization of PnBFD-M2

To verify the improvements in catalytic activity and thermal resistance of PnBFD-M2, its initial activity at varying FALD concentrations, half-life ($t_{1/2}$), optimal temperature (T_{opt}), and

storage stability at −20 °C, 4 °C and room temperature (RT, 22–25 °C) was determined.

The catalytic activities of PnBFD-M1 and PnBFD-M2 were evaluated and compared by measuring their initial reaction rates at FALD concentrations ranging from 10 to 200 mM at 37 °C. Because the formation of GALD from two FALD molecules proceeds *via* a ping-pong kinetic mechanism (Fig. S4),[41,55,74] the reaction cannot be adequately described by a conventional Michaelis–Menten model with a single set of k_{cat} and K_M values. The measurements at all tested FALD concentrations showed that the GALD concentration produced by PnBFD-M2 after 30 min is consistently higher than that of PnBFD-M1 (Fig. 4A, B and Fig. S5A–E). Moreover, this difference becomes more pronounced at elongated reaction times. For instance, at 100 mM FALD concentration after 7.5 h the GALD yield of PnBFD-M2 reached 3.92 mM compared to 2.48 mM produced by PnBFD-M1 (Fig. 4C). The lower yield of pnBFD-M1 compared to PnBFD-M2 is likely due to the lower thermal resistance, which leads to substantial enzyme inactivation after 40 min thereby slowing product accumulation. In contrast, PnBFD-M2 exhibits greater thermal resistance and therefore maintained activity for a longer period of time and allowing continued GALD production. At all FALD concentrations, PnBFD-M2 also displayed slightly higher initial rates for GALD production than PnBFD-M1 (Fig. 4D); at 200 mM FALD, the initial rate for GALD formation increased from 302.9 μmol per (min g protein) (PnBFD-M1) to 350.3 μmol per (min g protein) (PnBFD-M2), representing a 1.16-fold improvement. It should be noted that the increase in activity might be caused by the improved stability/thermal resistance, since it could result in a lower fraction of inactive enzymes during purification. On the basis that the maximal reaction rates of PnBFD-M1 and PnBFD-M2 are attained at approximately 200 mM FALD, a FALD concentration of around 100 mM can be estimated to correspond to half of the maximal activity (comparable to a K_M value).

The residual activity of PnBFD-M1 and PnBFD-M2 were measured after incubation at 37 °C, 40 °C, 45 °C, and 50 °C for various durations, and the corresponding $t_{1/2}$ were calculated. PnBFD-M1 exhibits rapid loss of activity at all tested temperatures, whereas PnBFD-M2 shows a slower rate of activity decline (Fig. 5A–D). The $t_{1/2}$ of PnBFD-M2 are longer than those of PnBFD-M1 at each tested temperature (Table 3). Notably, at 37 °C the $t_{1/2}$ of PnBFD-M2 increased to 2247 min, representing a 51-fold increase compared to PnBFD-M1 ($t_{1/2}$ (37 °C) = 44 min). The highly active GALS-YM has a reported T_m of 50.8 °C,[41] but its $t_{1/2}$ at 37 °C is less than 120 min under the tested conditions (Fig. S5F), therefore under these conditions PnBFD-M2 seems to be the more robust enzymes in spite of its slightly lower T_m.

The specific activity of PnBFD-M1 and PnBFD-M2 were measured over a temperature range of 25–60 °C, and their T_{opt}

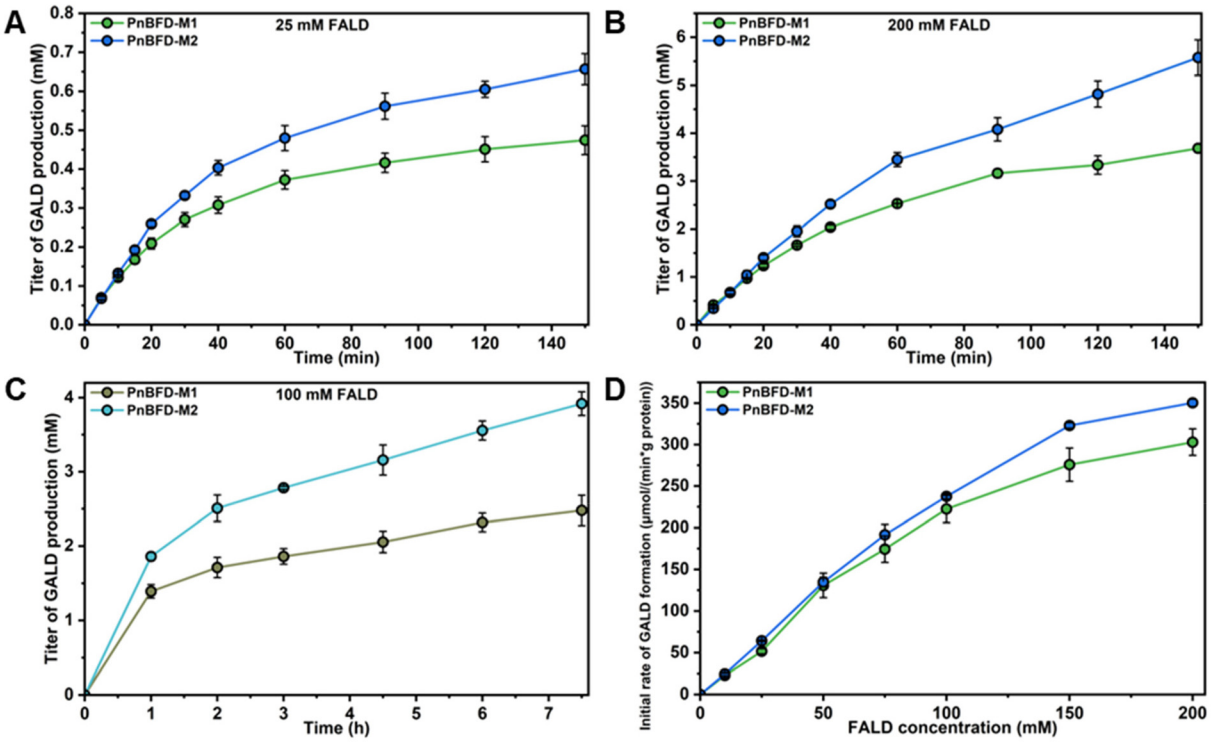

Fig. 4 (A) and (B) The GALD production of PnBFD-M1 and PnBFD-M2 at 25 mM and 200 mM FALD starting concentrations under 37 °C. (C) The GALD production of PnBFD-M1 and PnBFD-M2 at 100 mM FALD starting concentrations for 0–7.5 h under 37 °C. (D) The initial rate of GALD formation of PnBFD-M1 and PnBFD-M2 at 0–200 mM FALD starting concentrations. Activity assay: 50 mM bicine (pH 7.6), 300 mM NaCl, 1 mM TPP, 2 mM Mg^{2+}, 0.2 mg mL^{-1} purified enzyme, and 10–200 mM FALD concentration, 37 °C; the initial activity was calculated by fitting the linear area of the curve (first 20 min). Error bars represent standard deviation of three technical replicates (n = 3).

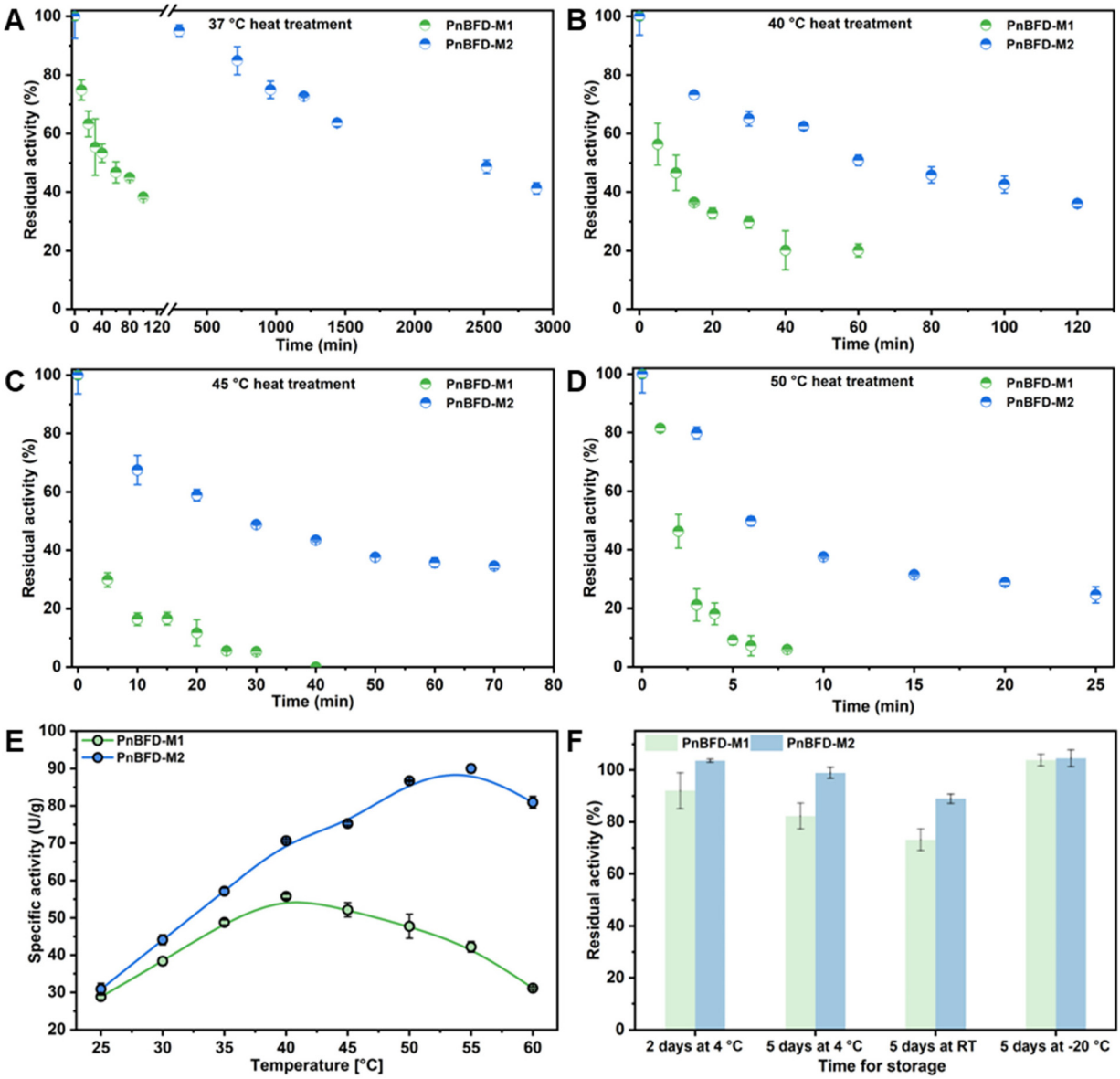

Fig. 5 (A)–(D) Residual activity of PnBFD-M1 and PnBFD-M2 after heat treatment at 37 °C, 40 °C, 45 °C, and 50 °C; 0.2 mg mL^{-1} PnBFD-M1 or PnBFD-M2 incubated at 37 °C, 40 °C, 45 °C, and 50 °C for different durations, after incubation the residual activity was measured, the activity of enzymes without heat treatment was set as 100%. (E) Specific activity of PnBFD-M1 and PnBFD-M2 at 25–60 °C and 10 mM FALD. Activity assay: 50 mM bicine (pH 7.6), 300 mM NaCl, 1 mM TPP, 2 mM Mg^{2+}, 0.2 mg mL^{-1} purified enzyme, and 10 mM FALD concentration, 25–60 °C for 30 min. The temperature at which the enzyme exhibits the highest activity is defined as T_{opt}. (F) The residual activity of PnBFD-M1 and PnBFD-M2 after storing at 4 °C, RT and −20 °C ; Error bars represent standard deviation of three technical replicates (n = 3).

were determined. Across all tested temperatures, PnBFD-M2 exhibits higher activity than PnBFD-M1 (Fig. 5E). The assays were performed using 10 mM FALD, a concentration well below the level that could cause substrate inhibition, ensuring that the observed differences reflect intrinsic thermal resistance rather than substrate effects. The highest specific activity of PnBFD-M2 (90.01 U g^{-1}) is 1.61-fold higher than that of PnBFD-M1 (55.76 U g^{-1}). PnBFD-M1 shows a T_{opt} of 40 °C with a narrow temperature tolerance; its activity drops below 80% when the reaction temperature exceeds 50 °C. In contrast, PnBFD-M2 displays a T_{opt} of 55 °C, which is 15 °C higher than that of PnBFD-M1, and a broader temperature tolerance, retaining 90% of its activity even at 60 °C. After storage at −20 °C for 5 days, both PnBFD-M1 and PnBFD-M2 fully retain their catalytic activity (Fig. 5F). After storage at 4 °C, the activity of PnBFD-M1 decreased to 92% after 2 days and further drop to 82.35% after 5 days, whereas PnBFD-M2 retains 99% of its activity after 5 days. After storage at RT for 5 days, the activity of PnBFD-M1 declined to 73%, while PnBFD-M2 still maintains 90% activity, indicating a significantly improved storage stability compared to PnBFD-M1. The operational stability of PnBFD-M2 was assessed over four consecutive reaction cycles

Table 3 $t_{1/2}$ of PnBFD-M1 and PnBFD-M2 at 37, 40, 45, and 50 °C

	$t_{1/2}$ (min)	
Temperature (°C)	PnBFD-M1	PnBFD-M2
37	44	2247
40	9.07	76
45	3.84	30
50	1.80	5.96

using a 30 kDa membrane for enzyme retention. Although PnBFD-M2 consistently exhibited higher retained activity than PnBFD-M1, a substantial decline in activity was observed upon reuse, with approximately 30% residual activity remaining after the fourth cycle (Fig. S6). This decrease cannot be attributed solely to enzyme loss *via* leakage or aggregation, as similar amounts of soluble protein were retained for both variants above the residual activity (PnBFD-M1: 67%; PnBFD-M2: 75%; Table S4), indicating progressive inactivation of the soluble enzyme. To evaluate substrate-induced deactivation, PnBFD-M2 was incubated with 500 mM FALD for 80 min at 4 °C to minimize thermal effects, retaining approximately 80% of its initial activity (data not show). These findings demonstrate that substrate-mediated deactivation limits operational lifetime and must be addressed in future optimization efforts, despite the improved intrinsic stability of PnBFD-M2.

PnBFD-M2 has a higher initial rate of GALD formation (350.3 μmol per (min g protein)), produces more GALD (3.92 mM), a prolonged $t_{1/2}$ (2247 min at 37 °C), a higher T_{opt} (55 °C), a broader temperature tolerance range, enhanced reusability, and improved storage stability at 4 °C (99% after 5 days) and RT (90% after 5 days) compared to PnBFD-M1 (at the same conditions). These characteristics indicate that PnBFD-M2 possesses enhanced thermal resistance and slightly increased catalytic activity compared to PnBFD-M1, making it one of the best enzymes to produce GALD from FALD.

Computer analysis of PnBFD-M2

MD simulations and analysis of the structure and dynamics of PnBFD-M2 were performed to gain insights in the increased thermal resistance and activity. MD simulations were conducted on PnBFD-M1 and PnBFD-M2, with three 100 ns trajectories simulated for each enzyme. Instead of TPP the FALD-TPP intermediate was chosen, since it is reported that the aldol condensation of a second FALD with the FALD-TPP is the rate limiting step and therefore for the GALD production of most interest.[75] The quantitative analysis of the change in hydrophobicity of the protein surface was done using reported amino acid hydrophobicity values.[76] MD simulations were utilized to explore the flexibility of side chains, and the change of secondary structures to provide key insights into the factors contributing to thermal resistance and activity improvement.

Analysis of RMSF of the variants revealed that PnBFD-M2 exhibits in the residue regions 171–180, 188–193, 233–235, 284–285, 331–333, and 394–401 lower RMSF values compared to PnBFD-M1 (RMSD of the Cα atoms was seen in Fig. S3B and Fig. 6A). Except for residues 188–193, all these segments are located in loop regions (Fig. 6B). The reduced flexibility of these regions contributes to enhanced structural rigidity, thereby likely improving thermal resistance. The residues 171–180, 233–235, and 394–401 are located near the active site. Although 171–180, 233–235, and 394–401 loop regions are spatially distant from the mutation sites K188I, Q192I, and A282P, the reduced flexibility observed in these regions may be attributed to long-range effects induced by the mutations.

The decreased flexibility in the 233–235 and 394–401 loop regions may help to stabilize substrate binding, which could account for the observed increase in enzymatic activity. The calculated values of hydrogen bonds (H-bonds), radius of gyration (R_g), and solvent-accessible surface area (SASA) for PnBFD-M1 and PnBFD-M2 show minimal differences (Fig. S7), suggesting that the overall structural compactness and solvent exposure remain largely unchanged between PnBFD-M1 and PnBFD-M2.

Analysis of the hydrophobicity of the protein surface showed that the K188I and Q192I substitutions in PnBFD-M2 are able to form hydrophobic interactions with adjacent residues V187 and L325 (Fig. 6C and D), which enhances intramolecular hydrophobic interactions, thereby likely improving thermal resistance.

MD simulations and analysis of the hydrophobicity of the surface indicate that the reduced protein flexibility, and increased hydrophobic interface of the helix (185–196) are key contributors to the improved thermal resistance of PnBFD-M2. The decreased flexibility of active-site loops 394–401 and 233–235 might also further promote enzymatic activity, in agreement with our previous finding showing that reduced flexibility of these same loops enhances catalytic performance.[41]

Construction of L-xylose pathway using FALD as sole feedstock

A one-pot reaction system was established for the production of L-xylose from FALD as the sole feedstock with PnBFD-M2 and FSA-TG. Since PnBFD-M2 has a higher thermal resistance compared to PnBFD-M1, the use of PnBFD-M2 should result in higher yields and thereby showing the potential of PnBFD-M2 for usage in enzymes cascades. PnBFD (to produce GALD) and FSA-TG (to produce GCA) both utilized FALD as a substrate, therefore the ratio of both enzymes and the absolute amount needed to be optimized.

Various enzyme mass ratios of PnBFD-M2 to FSA-TG (2 : 1 (1 : 1.2), 4 : 1 (1: 0.6), 2 : 2 (1 : 2.4), and 4 : 2 (1 : 1.2), corresponding to molar ratios in brackets) with 100 mM initial FALD concentration were tested for L-xylose production (Fig. 7). The by-products GALD (left over intermediate) and erythrose remain at low levels across all tested enzyme ratios. Increasing the amount of FSA-TG effectively reduces the concentration of the by-product threose, and its level further decreases over time.

The drop of measured threose with increasing levels of FSA-TG, which was also reported,[29] can be explained by the fact that FSA-TG can catalyze the condensation of threose with

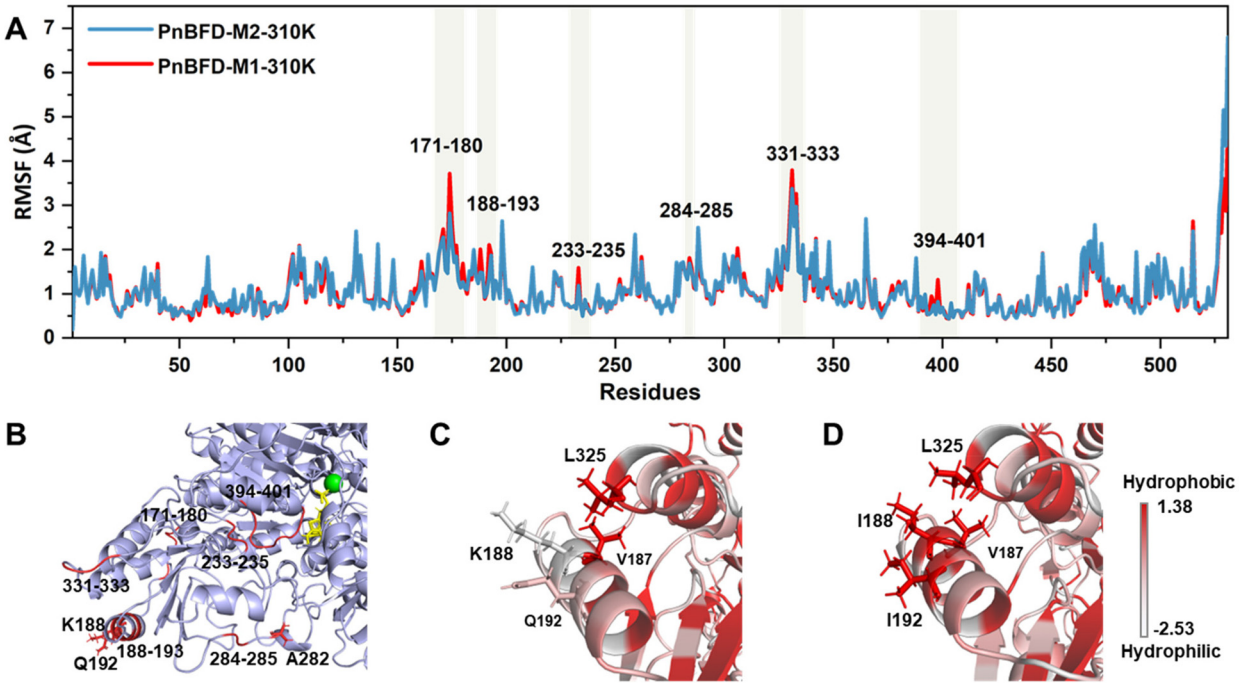

Fig. 6 (A) RMSF (50–100 ns) of PnBFD-M1 and PnBFD-M2 at 310K. (B) Partial structure of the PnBFD-M1 dimer. Mg^{2+} is shown as green spheres, and the TPP-FALD complex is represented as yellow sticks. Regions with higher RMSF in PnBFD-M1 compared to PnBFD-M2 are highlighted in red cartoon. Residues K188, Q192, and A282 are shown as red sticks. Model of the (C) PnBFD-M1 and (D) PnBFD-M2 visualize the hydrophobicity around positions 188 and 192. PnBFD-M2 shows that the hydrophobicity substitutions of 188 and 192 positions can form hydrophobic interactions with V187 and L325, enhance the hydrophobicity of the protein surface, which indicates that hydrophobicity is the main driver in improving thermal resistance performance. K188, Q192, V187, L325, I188, and I192 were shown as sticks; Higher scores indicating greater hydrophobicity.

FALD to form xylose, but it cannot condense erythrose with FALD (Fig. S8). Raising the concentration of PnBFD-M2 significantly enhanced L-xylose production and FALD conversion, whereas a higher amount of FSA-TG led to only a slight improvement in L-xylose. These results indicate that the L-xylose production is more dependent on PnBFD-M2 levels (Fig. 7A *vs.* C compared to Fig. 7A *vs.* B) under the tested conditions. In all measurements GCA levels remained high, indicating that the optimal balance between PnBFD-M2 and FAS-TG and the total amount of enzymes needs to be further optimized. As shown in Fig. 7A *vs.* C, too much excess of PnBFD-M2 led to the accumulation of threose and erythrose, indicating that the condensation of GALD with GCA by FSA-TG is a limiting factor.

Subsequently, higher amounts of enzymes and partly altered ratios (PnBFD-M2 : FSA-TG = 6 : 3 (1 : 1.2) and 6 : 4 (1 : 1.6), molar ratios in brackets) were evaluated. At a ratio of 6 : 4, the L-xylose concentration reached 14.12 mM (Fig. S9A and B). However, FALD is not completely consumed, and by-product levels remain relatively high. With 8 mg mL^{-1} PnBFD-M2 (134 μM) and 4 mg mL^{-1} (162 μM) FSA-TG after 10 h a L-xylose yield of 15.17 mM was obtained (Fig. 8A), higher amounts of PnBFD-M2 did not further show improved yields (Fig. S9C). At this point, the substrate FALD is nearly exhausted (0.98 mM), and the levels of by-products GALD, threose, and erythrose were all significantly reduced and the GCA concentration dropped to 6.13 mM.

After determining the optimal enzyme mass ratio of PnBFD-M2 to FSA-TG to be 8 : 4 (molar ration 1 : 1.2) the reaction temperature was optimized (40 °C, 45 °C, and 50 °C) (Fig. 8B, C and Fig. S9B). At 40 °C, the highest L-xylose yield was achieved, reaching 15.70 mM (2.36 g L^{-1}), with a conversion efficiency of 78%. At this temperature, the substrate FALD and by-products GALD, threose, and erythrose remain at low levels, and the concentration of GCA was 6.80 mM. At higher temperatures (45 °C and 50 °C), the concentration of FALD decreased within 2 h to ~5 mM, indicating that PnBFD-M2 retained catalytic activity at elevated temperatures (Fig. 8C and Fig. S9D). However, the L-xylose yield declined under these conditions, likely because increased temperature enhanced the activity of FSA-TG toward threose formation more than toward the synthesis of GCA and L-xylose, resulting in higher threose accumulation (Fig. 8C and Fig. S9D). The L-xylose production of reactions with PnBFD-M1 at the same enzyme concentration as PnBFD-M2 was also evaluated across different temperatures (Fig. 8D, E and Fig. S9D–F). At all tested temperatures, cascades with PnBFD-M1 yielded lower amounts of L-xylose and the FALD concentration did not drop as low as with PnBFD-M2, indicating a more rapid loss of activity for PnBFD-M1. Notably, in reactions with PnBFD-M1, the residual

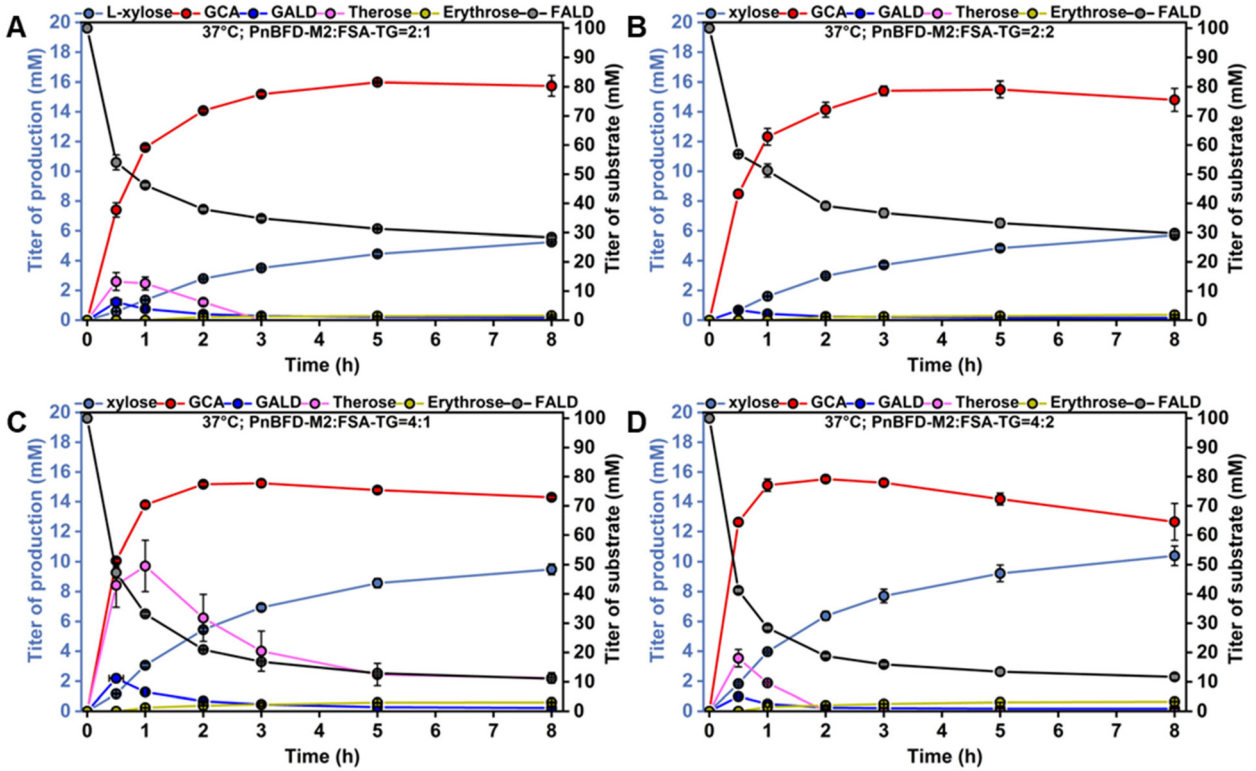

Fig. 7 Titer of products and substrate in L-xylose pathway with different ratio of PnBFD-M2 and FSA-TG. (A) 37 °C, 2 mg mL^{-1} PnBFD-M2 and 1 mg mL^{-1} FSA-TG. (B) 37 °C, 2 mg mL^{-1} PnBFD-M2 and 2 mg mL^{-1} FSA-TG. (C) 37 °C, 4 mg mL^{-1} PnBFD-M2 and 1 mg mL^{-1} FSA-TG. (D) 37 °C, 4 mg mL^{-1} PnBFD-M2 and 2 mg mL^{-1} FSA-TG. Activity assay: 50 mM pH7.6 bicine, 300 mM NaCl, 1 mM TPP, 2 mM Mg^{2+}, purified enzymes, and 100 mM FALD concentration, 37 °C for 8 h. Error bars represent standard deviation of three technical replicates (n = 3).

FALD concentration remained at ~10 mM after 2 h at 45 °C and as high as ~15 mM at 50 °C (Fig. 8E and Fig. S9F), whereas in reactions with PnBFD-M2, it consistently decreased to ~5 mM under the same conditions (Fig. 8B and Fig. S9D). This behaviour can be attributed to the lower thermal resistance of PnBFD-M1, which leads to a more rapid decline in catalytic activity at elevated temperatures. The highest L-xylose titer by PnBFD-M1 occurred at 37 °C, reaching 11.76 mM (1.76 g L^{-1}, a relative yield of 58.80%) (Fig. S9E), which is lower than that of PnBFD-M2 at the same temperature (15.17 mM) and also lower than the highest yield achieved by PnBFD-M2 (15.70 mM at 40 °C, 2.36 g L^{-1}). Additionally, the L-xylose yield of PnBFD-M1 decreased progressively with increasing temperature. These results suggest that enhancing the thermal resistance and moderately improving the activity of PnBFD-M1 was beneficial for the production of L-xylose in the presented enzyme cascade.

For product mass determination, the reaction was scaled up to 38 mL using 8 mg mL^{-1} PnBFD-M2 and 4 mg mL^{-1} FSA-TG. A L-xylose concentration of 10.01 mM was obtained after 10 h at 40 °C, corresponding to a total product amount of approximately 57.11 mg, which is in a similar range as the small-scale production but not as high (best conditions reached about 16 mM). A portion of the product was isolated by HPLC, and the product peak was collected manually and subsequently analyzed by mass spectrometry (MS) (Fig. S10), confirming the molecular mass of L-xylose. Of theoretical 57.11 mg L-xylose, 47 mg L-xylose (82%) were recovered with a purity of 79%. The formation of L-xylose by FSA-TG has previously been verified by NMR spectroscopy.[29]

The one-pot enzymatic cascade combining PnBFD-M2 and FSA-TG enables the conversion of FALD to L-xylose without the need for costly redox cofactors such as nicotinamide adenine dinucleotide (NADH) or nicotinamide adenine dinucleotide phosphate (NADPH). This cofactor-independent system represents a conceptually attractive route for L-xylose production, and the low levels of side products formed (GALD, threose, and erythrose) are expected to be separable using established sugar purification technologies, including ion-exchange and simulated moving bed chromatography.[77,78]

Nevertheless, the current system remains far from industrial implementation and should primarily be regarded as a proof of concept demonstrating the potential of engineered benzoylformate decarboxylases, such as PnBFD-M2, for FALD valorisation. The use of FALD in enzymatic processes remains challenging due to its high reactivity, as reflected by the gradual loss of activity observed for PnBFD-M2 despite its enhanced thermal stability relative to PnBFD-M1. Although the simultaneous engineering of thermal robustness and FALD tolerance would be desirable, such multidimensional optimi-

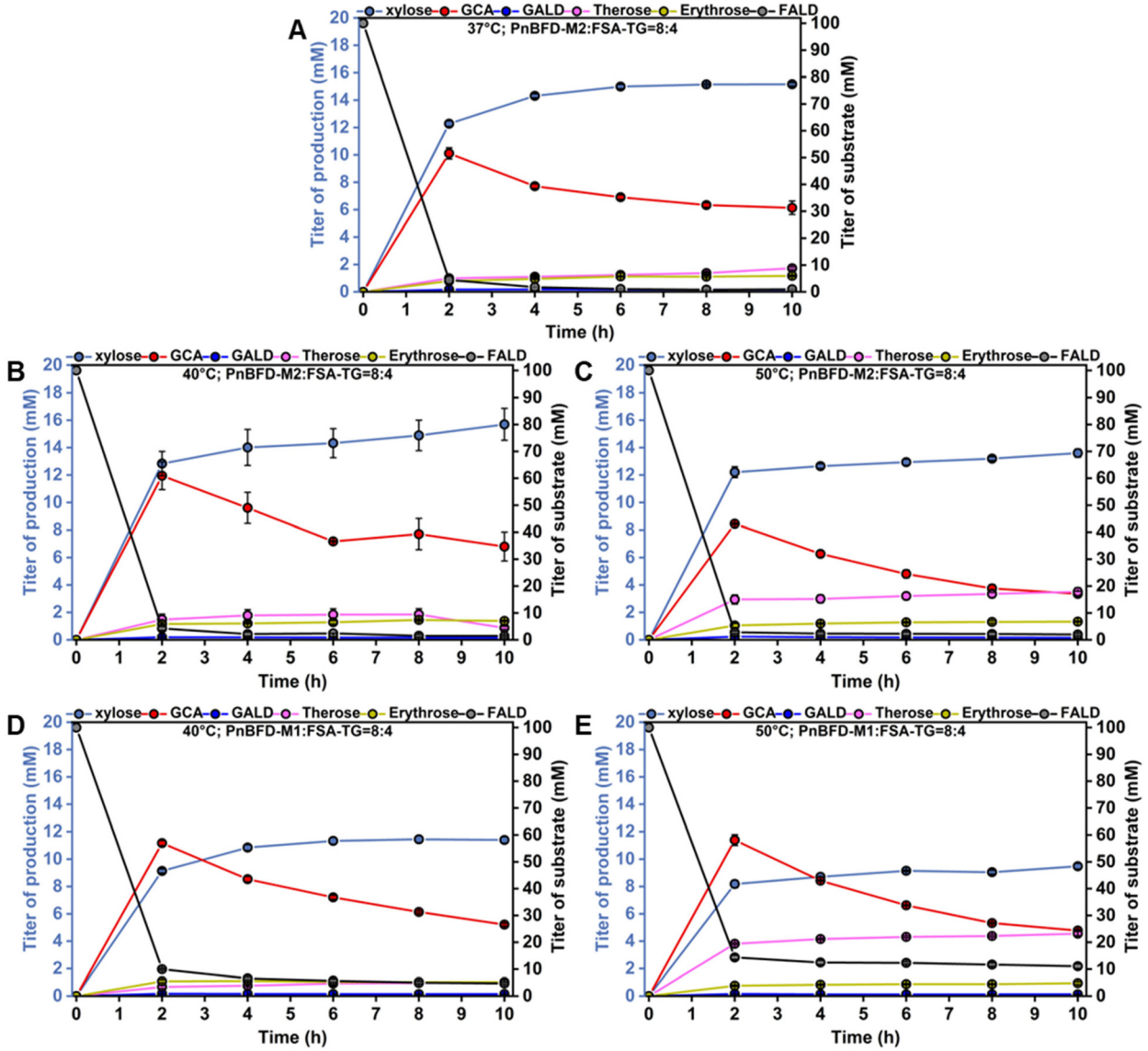

Fig. 8 Titer of products and substrate in L-xylose pathway with PnBFD-M2 or PnBFD-M1 and FSA-TG at different temperature. (A) 37 °C, 8 mg mL^{-1} PnBFD-M2 and 4 mg mL^{-1} FSA-TG. (B) 40 °C, 8 mg mL^{-1} PnBFD-M2 and 4 mg mL^{-1} FSA-TG. (C) 50 °C, 8 mg mL^{-1} PnBFD-M2 and 4 mg mL^{-1} FSA-TG. (D) 40 °C, 8 mg mL^{-1} PnBFD-M1 and 4 mg mL^{-1} FSA-TG. (E) 50 °C, 8 mg mL^{-1} PnBFD-M1 and 4 mg mL^{-1} FSA-TG. Activity assay: 50 mM pH7.6 bicine, 300 mM NaCl, 1 mM TPP, 2 mM Mg^{2+}, purified enzyme, and 100 mM FALD concentration, different temperature for 10 h. Error bars represent standard deviation of three technical replicates (n = 3).

sation is inherently limited by the low probability of identifying optimal mutation combinations in a single step. The improved stability of PnBFD-M2 therefore provides a suitable starting point for targeted engineering efforts aimed at enhancing tolerance towards FALD. In this context, detailed studies on the mechanisms of FALD-induced deactivation would be valuable and broadly beneficial to the field.

While the one-pot cascade is attractive due to its simplicity and conceptually supports the feasibility of *in vivo* implementation (with a single cell approximated as a one-pot system), several factors currently limit its overall yield. A key limitation arises from substrate competition within the cascade, as both for FALD and GALD participate in multiple reaction steps, combined with imbalanced reaction rates of FSA-TG toward GCA and L-xylose formation. Under all conditions tested (Fig. 7 and 8), FSA-TG preferentially converts substrates to GCA, leading to rapid GCA accumulation and depletion of GALD, which is required for L-xylose formation. This imbalance ultimately constrains L-xylose productivity.

Adjusting the enzyme ratio can partially mitigate this effect; however, the inherently higher catalytic efficiency of FSA-TG toward GCA formation imposes a fundamental limitation on optimisation within a single-pot setup. To overcome this constraint, spatial separation of the cascade steps, for example in a flow reactor with compartmentalised enzyme zones, could provide improved control over intermediate fluxes. In such a

system, GALD formation, GCA production, and L-xylose synthesis could be distributed across discrete reaction zones, enabling independent optimisation of residence time, enzyme loading, and intermediate concentrations, which is not accessible in a one-pot setup.

Alternatively, pathway decoupling through the use of engineered FSA variants with selectively enhanced activity toward either GCA or L-xylose formation could further reduce substrate competition. While this strategy would require additional protein engineering efforts and increase process complexity and cost by introducing an additional enzyme, it represents a viable long-term approach to improve selectivity and overall cascade efficiency.

Conclusions

By targeting the structural domain of PnBFD-M1 using ΔΔ*G*-guided virtual screening and proline substitutions in flexible loops, we generated a significantly improved variant, PnBFD-M2. This enzyme displays markedly enhanced thermal resistance (T_m +11.2 °C; $t_{1/2}$ at 37 °C extended from 44 min to 2247 min) and slightly improved catalytic activity (GALD formation increased from 302.9 to 350.3 μmol per(min g protein)), demonstrating that both design strategies can be combined to effectively enhance stability without compromising function. PnBFD-M2 ranks among the most efficient GALD-from-FALD producing enzymes reported, with <1% DHA formation and superior thermal robustness compared with GALS-YM[41] ($t_{1/2}$ < 120 min). When combined with FSA-TG, PnBFD-M2 enabled a one-pot synthesis of L-xylose from FALD as the sole feedstock, increasing product titers from 1.76 to 2.36 g L^{-1} due to its improved activity and stability.

In conclusion, with a T_m of 49.2 °C, an initial activity of 350.3 μmol per (min g protein), and low by-product formation, PnBFD-M2 is a promising biocatalyst for the efficient FALD-to-GALD conversion. Its robustness and selectivity position it as an attractive component for multi-enzyme cascades that valorize renewable C1 intermediates, supporting greener routes for CO_2-based biochemical production.

Author contributions

J. Z. performed the experiments and wrote the manuscript. F. B. designed the experiments, contributed to data analysis, and revised the manuscript. T. T. and U. S. conceived and designed the experiments and revised the manuscript. All the authors read and approved the final manuscript.

Conflicts of interest

The authors declare no conflict of interests.

Data availability

Supplementary information (SI): data relating to the methods, experimental procedures, and other supplemental results. See DOI: https://doi.org/10.1039/d5gc06542a.

Acknowledgements

Junhui Zhou was supported by a Ph.D. scholarship from the China Scholarship Council (CSC No. 202106880007). This work was financially supported by the National Key R&D Program of China (Grant No. 2023YFB4203500) and the Natural Science Foundation of China (NSFC) (U24A6011). Calculations were performed with computing resources granted by HPC from RWTH Aachen University under projects rwth1689. Special thanks go to Dr Ziheng Cui for assistance with computer analysis and figure improvements. Special thanks go to Petra Esser from the DWI – Leibniz Institute for Interactive Materials for conduction the MS measurements.

References

1 P. Izadi and F. Harnisch, Microbial | electrochemical CO_2 reduction: To integrate or not to integrate?, *Joule*, 2022, **6**(5), 935–940.
2 T. Zheng, M. Zhang, L. Wu, S. Guo, X. Liu, J. Zhao, W. Xue, J. Li, C. Liu, X. Li, Q. Jiang, J. Bao, J. Zeng, T. Yu and C. Xia, Upcycling CO_2 into energy-rich long-chain compounds via electrochemical and metabolic engineering, *Nat. Catal.*, 2022, **5**(5), 388–396.
3 X. Liu, H. Luo, D. Yu, J. Tan, J. Yuan and H. Li, Synthetic biology promotes the capture of CO_2 to produce fatty acid derivatives in microbial cell factories, *Bioresour. Bioprocess.*, 2022, **9**(1), 124.
4 S. Bierbaumer, M. Nattermann, L. Schulz, R. Zschoche, T. J. Erb, C. K. Winkler, M. Tinzl and S. M. Glueck, Enzymatic conversion of CO_2: From natural to artificial utilization, *Chem. Rev.*, 2023, **123**(9), 5702–5754.
5 K. Nakata, T. Ozaki, C. Terashima, A. Fujishima and Y. Einaga, High-yield electrochemical production of formaldehyde from CO_2 and seawater, *Angew. Chem., Int. Ed.*, 2014, **53**(3), 871–874.
6 S. Zhao, H. Q. Liang, X. M. Hu, S. Li and K. Daasbjerg, Challenges and prospects in the catalytic conversion of carbon dioxide to formaldehyde, *Angew. Chem., Int. Ed.*, 2022, **61**(46), e202204008.
7 Z. Li, P. Wang, G. Han, S. Yang, S. Roy, S. Xiang, J. D. Jimenez, V. K. R. Kondapalli, X. Lyu, J. Li, A. Serov, R. Li, V. Shanov, S. D. Senanayake, A. I. Frenkel, P. M. Ajayan, Y. Sun, T. P. Senftle and J. Wu, Ampere-level co-electrosynthesis of formate from CO_2 reduction paired with formaldehyde dehydrogenation reactions, *Nat. Commun.*, 2025, **16**(1), 4850.

8 W. H. Wang, Y. Himeda, J. T. Muckerman, G. F. Manbeck and E. Fujita, CO_2 hydrogenation to formate and methanol as an alternative to photo- and electrochemical CO_2 reduction, *Chem. Rev.*, 2015, **115**(23), 12936–12973.

9 Y. Wang, E. Chen and J. Tang, Insight on reaction pathways of photocatalytic CO_2 conversion, *ACS Catal.*, 2022, **12**(12), 7300–7316.

10 A. Rodil, J. Deska and M. H. G. Prechtl, Formaldehyde and its surrogates as a C1 platform for defossilised modern societies, *Chem. Soc. Rev.*, 2025, **54**(24), 11398–11422.

11 H. Varela, E. A. Paredes-Salazar, F. H. B. Lima and K. Eid, Renewable methanol and the energy challenge: The role of electrocatalysis, *Curr. Opin. Electrochem.*, 2024, **46**, 101539.

12 L. E. Heim, H. Konnerth and M. H. G. Prechtl, Future perspectives for formaldehyde: pathways for reductive synthesis and energy storage, *Green Chem.*, 2017, **19**(10), 2347–2355.

13 A. I. Benitez-Mateos, D. R. Padrosa and F. Paradisi, Multistep enzyme cascades as a route towards green and sustainable pharmaceutical syntheses, *Nat. Chem.*, 2022, **14**(5), 489–499.

14 T. Cai, H. Sun, J. Qiao, L. Zhu, F. Zhang, J. Zhang, Z. Tang, X. Wei, J. Yang, Q. Yuan, W. Wang, X. Yang, H. Chu, Q. Wang, C. You, H. Ma, Y. Sun, Y. Li, C. Li, H. Jiang, Q. Wang and Y. Ma, Cell-free chemoenzymatic starch synthesis from carbon dioxide, *Science*, 2021, **373**(6562), 1523–1527.

15 X. Lu, Y. Liu, Y. Yang, S. Wang, Q. Wang, X. Wang, Z. Yan, J. Cheng, C. Liu, X. Yang, H. Luo, S. Yang, J. Gou, L. Ye, L. Lu, Z. Zhang, Y. Guo, Y. Nie, J. Lin, S. Li, C. Tian, T. Cai, B. Zhuo, H. Ma, W. Wang, Y. Ma, Y. Liu, Y. Li and H. Jiang, Constructing a synthetic pathway for acetyl-coenzyme A from one-carbon through enzyme design, *Nat. Commun.*, 2019, **10**(1), 1378.

16 X. Wang, H. Luo, Y. Wang, Y. Wang, T. Tu, X. Qin, X. Su, H. Huang, Y. Bai, B. Yao and J. Zhang, Direct conversion of carbon dioxide to glucose using metabolically engineered, *Cupriavidus necator*, *Bioresour. Technol.*, 2022, **362**, 127806.

17 J. Zhang, D. Liu, Y. Liu, H. Chu, J. Bai, J. Cheng, H. Zhao, S. Fu, H. Liu, Y. Fu, Y. Ma and H. Jiang, Hybrid synthesis of polyhydroxybutyrate bioplastics from carbon dioxide, *Green Chem.*, 2023, **25**(8), 3247–3255.

18 H.-J. Jo, J.-H. Kim, Y.-N. Kim, P.-W. Seo, C.-Y. Kim, J.-W. Kim, H.-n. Yu, H. Cheon, E. Y. Lee, J.-S. Kim and J.-B. Park, Glyoxylate carboligase-based whole-cell biotransformation of formaldehyde into ethylene glycol via glycolaldehyde, *Green Chem.*, 2022, **24**(1), 218–226.

19 J. Zhou, X. Tian, Q. Yang, Z. Zhang, C. Chen, Z. Cui, Y. Ji, U. Schwaneberg, B. Chen and T. Tan, Three multi-enzyme cascade pathways for conversion of C1 to C2/C4 compounds, *Chem Catal.*, 2022, **2**(10), 2675–2690.

20 H.-J. Jo, H. Yu, H. Cheon, J.-H. Kim, G. Y. Kim, B. S. Kim, J.-S. Kim and J.-B. Park, Multilayer engineering of an *escherichia coli*-based biotransformation system to exclusively produce glycolic acid from formaldehyde, *ACS Sustainable Chem. Eng.*, 2023, **11**(3), 1078–1086.

21 J. H. Kim, H. Cheon, H. J. Jo, J. W. Kim, G. Y. Kim, H. R. Seo, P. W. Seo, J. S. Kim and J. B. Park, Engineering of two thiamine diphosphate-dependent enzymes for the regioselective condensation of C1-formaldehyde into C4-erythrulose, *Int. J. Biol. Macromol.*, 2023, **253**(Pt 8), 127674.

22 V. P. Willers, M. Döring, B. Beer and V. Sieber, Cell-free enzymatic L-alanine synthesis from green methanol, *Chem Catal.*, 2023, **3**(3), 100502.

23 J. Yang, W. Song, T. Cai, Y. Wang, X. Zhang, W. Wang, P. Chen, Y. Zeng, C. Li, Y. Sun and Y. Ma, De novo artificial synthesis of hexoses from carbon dioxide, *Sci. Bull.*, 2023, **68**(20), 2370–2381.

24 Y. Wu, G. Lu, R. Zeng, Z. Li, X. Xu, Y. Gui, C. Guo, L. Deng, Y. Bie, D. Zhang, Y. He, Y. He, Y. Zhu, C. Fu and L. Yu, Innovative coupling pathway for second- and third-generation biomass: Efficient L-lactate synthesis from xylose and C1 compounds, *Chem. Eng. J.*, 2025, **505**, 159573.

25 X.-W. Ding, J. Rong, Z.-P. Pan, X.-X. Zhu, Z.-Y. Zhu, Q. Chen, Z.-J. Zhang, J.-H. Xu, C.-X. Li and G.-W. Zheng, De novo multienzyme synthetic pathways for lactic acid production, *ACS Catal.*, 2024, 4665–4674.

26 Y. Yan, H. Zhao, D. Liu, J. Zhang, Y. Liu and H. Jiang, Redesigning glycolaldehyde synthase for the synthesis of biorefinery feedstock D-xylulose from C1 compounds, *Biotechnol. J.*, 2024, **19**(9), e2400360.

27 S. Gong, T. Li, Z. Tang, Z. Tan, R. Zhang, K. Olsen, H. Liu and L. Zhu, One-pot enzymatic synthesis of L-threitol from C1 formaldehyde, *Green Chem.*, 2025, **27**(8), 2189–2196.

28 M. Jia, M. Liu, J. Li, W. Jiang, F. Xin, W. Zhang, Y. Jiang and M. Jiang, Formaldehyde: An essential intermediate for C1 metabolism and bioconversion, *ACS Synth. Biol.*, 2024, **13**(11), 3507–3522.

29 A. Szekrenyi, X. Garrabou, T. Parella, J. Joglar, J. Bujons and P. Clapes, Asymmetric assembly of aldose carbohydrates from formaldehyde and glycolaldehyde by tandem biocatalytic aldol reactions, *Nat. Chem.*, 2015, **7**(9), 724–729.

30 Q. Meng, T. Zhang, B. Jiang, W. Mu and M. Miao, Advances in applications, metabolism, and biotechnological production of L-xylulose, *Appl. Microbiol. Biotechnol.*, 2016, **100**(2), 535–540.

31 A. Usvalampi, O. Turunen, J. Valjakka, O. Pastinen, M. Leisola and A. Nyyssölä, Production of L-xylose from L-xylulose using Escherichia coli L-fucose isomerase, *Enzyme Microb. Technol.*, 2012, **50**(1), 71–76.

32 C. Wang, C. Fan, Z. Zhang, Z. Zhu, C. Wu and T. Sun, Synthesis, crystal structure, spectral analysis, DFT calculations, docking studies, in vitro biological activity evaluation and in silico drug-likeness prediction of a novel L-xylose derivative, *J. Mol. Struct.*, 2023, **1294**, 136362.

33 J.-B. Behr and G. Guillerm, A concise synthesis of 2,5-dideoxy-2,5-imino-d-mannitol (DMDP) and HomoDMDP from L-xylose, *Tetrahedron Lett.*, 2007, **48**(13), 2369–2372.

34 E. Moyroud and P. Strazewski, L-ribonucleosides from L-xylose, *Tetrahedron*, 1999, **55**(5), 1277–1284.

35 W.-B. Yang, S. S. Patil, C.-H. Tsai, C.-H. Lin and J.-M. Fang, The synthesis of L-gulose and L-xylose from D-gluconolactone, *Tetrahedron*, 2002, **58**(2), 253–259.

36 T. B. Granström, G. Takata, K. Morimoto, M. Leisola and K. Izumori, L-Xylose and, L-lyxose production from xylitol using *Alcaligenes 701B* strain and immobilized L-rhamnose isomerase enzyme, *Enzyme Microb. Technol.*, 2005, **36**(7), 976–981.

37 J. J. Forsman and R. Leino, L-Pentoses, in biological and medicinal applications, *Chem. Rev.*, 2011, **111**(5), 3334–3357.

38 E. Dimant and M. Banay, Notes- Preparation of L-Xylose, *J. Org. Chem.*, 1960, **25**(3), 475–476.

39 J. B. Siegel, A. L. Smith, S. Poust, A. J. Wargacki, A. Bar-Even, C. Louw, B. W. Shen, C. B. Eiben, H. M. Tran, E. Noor, J. L. Gallaher, J. Bale, Y. Yoshikuni, M. H. Gelb, J. D. Keasling, B. L. Stoddard, M. E. Lidstrom and D. Baker, Computational protein design enables a novel one-carbon assimilation pathway, *Proc. Natl. Acad. Sci. U. S. A.*, 2015, **112**(12), 3704–3709.

40 S. Güner, V. Wegat, A. Pick and V. Sieber, Design of a synthetic enzyme cascade for the in vitro fixation of a C1 carbon source to a functional C4 sugar, *Green Chem.*, 2021, **23**(17), 6583–6590.

41 J. Zhou, F. Bourdeaux, V. Emann, T. Tan and U. Schwaneberg, A highly active and specific benzoylformate decarboxylase for glycolaldehyde production from formaldehyde, *ACS Catal.*, 2025, 14469–14482.

42 N. J. Claassens, S. Burgener, B. Vogeli, T. J. Erb and A. Bar-Even, A critical comparison of cellular and cell-free bioproduction systems, *Curr. Opin. Biotechnol.*, 2019, **60**, 221–229.

43 K. Xu, Q. Chen, H. Fu, Q. Chen, J. Gu, X. Wang and J. Zhou, Simultaneous engineering of the thermostability and activity of a novel aldehyde dehydrogenase, *ACS Catal.*, 2025, **15**(3), 1841–1853.

44 A. Karshikoff, L. Nilsson and R. Ladenstein, Rigidity versus flexibility: the dilemma of understanding protein thermal stability, *FEBS J.*, 2015, **282**(20), 3899–3917.

45 L. Zhu, F. Cheng, V. Piatkowski and U. Schwaneberg, Protein engineering of the antitumor enzyme PpADI for improved thermal resistance, *ChemBioChem*, 2014, **15**(2), 276–283.

46 Z. Huang, J. Zhou, J. Wang, S. Xu, C. Cheng, J. Ma and Z. Gao, Complementary distant and active site mutations simultaneously enhance catalytic activity and thermostability of α-galactosidase, *J. Agric. Food Chem.*, 2025, **73**(6), 3635–3644.

47 N. G. Nezhad, R. N. Z. R. A. Rahman, Y. M. Normi, S. N. Oslan, F. M. Shariff and T. C. Leow, Thermostability engineering of industrial enzymes through structure modification, *Appl. Microbiol. Biotechnol.*, 2022, **106**(13), 4845–4866.

48 H. Xing, G. Zou, C. Liu, S. Chai, X. Yan, X. Li, R. Liu, Y. Yang and Z. Zhou, Improving the thermostability of a GH11 xylanase by directed evolution and rational design guided by *B*-factor analysis, *Enzyme Microb. Technol.*, 2021, **143**, 109720.

49 E. L. Bell, R. Smithson, S. Kilbride, J. Foster, F. J. Hardy, S. Ramachandran, A. A. Tedstone, S. J. Haigh, A. A. Garforth, P. J. R. Day, C. Levy, M. P. Shaver and A. P. Green, Directed evolution of an efficient and thermostable PET depolymerase, *Nat. Catal.*, 2022, **5**(8), 673–681.

50 N. G. Nezhad, R. N. Z. R. A. Rahman, Y. M. Normi, S. N. Oslan, F. M. Shariff and T. C. Leow, Recent advances in simultaneous thermostability-activity improvement of industrial enzymes through structure modification, *Int. J. Biol. Macromol.*, 2023, **232**, 123440.

51 C. Chen, B.-H. Guan, Q. Geng, Y.-C. Zheng, Q. Chen, J. Pan and J.-H. Xu, Enhanced thermostability of *Candida* ketoreductase by computation-based cross-regional combinatorial mutagenesis, *ACS Catal.*, 2023, **13**(11), 7407–7416.

52 M. Rahban, S. Zolghadri, N. Salehi, F. Ahmad, T. Haertlé, N. Rezaei-Ghaleh, L. Sawyer and A. A. Saboury, Thermal stability enhancement: Fundamental concepts of protein engineering strategies to manipulate the flexible structure, *Int. J. Biol. Macromol.*, 2022, **214**, 642–654.

53 A. Huang, C. Chai, J. Zhang, L. Zhao, F. Lu and F. Liu, Engineered N57P variant of ulvan lyase with improvement of catalytic efficiency and thermostability via reducing loop flexibility and anchoring substrate, *ACS Sustainable Chem. Eng.*, 2021, **9**(48), 16415–16423.

54 C. S. Karamitros, K. Murray, B. Winemiller, C. Lamb, E. M. Stone, S. D'Arcy, K. A. Johnson and G. Georgiou, Leveraging intrinsic flexibility to engineer enhanced enzyme catalytic activity, *Proc. Natl. Acad. Sci. U. S. A.*, 2022, **119**(23), e2118979119.

55 S. Liu, X. Gong, X. Yan, T. Peng, J. C. Baker, L. Li, P. M. Robben, S. Ravindran, L. A. Andersson, A. B. Cole and T. E. Roche, Reaction mechanism for mammalian pyruvate dehydrogenase using natural lipoyl domain substrates, *Arch. Biochem. Biophys.*, 2001, **386**(2), 123–135.

56 G. Qu, Y. Bi, B. Liu, J. Li, X. Han, W. Liu, Y. Jiang, Z. Qin and Z. Sun, Unlocking the stereoselectivity and substrate acceptance of enzymes: proline-induced loop engineering test, *Angew. Chem., Int. Ed.*, 2022, **61**(1), e202110793.

57 A. Remeeva, V. V. Nazarenko, I. M. Goncharov, A. Yudenko, A. Smolentseva, O. Semenov, K. Kovalev, C. Gülbahar, U. Schwaneberg, M. D. Davari, V. Gordeliy and I. Gushchin, Effects of proline substitutions on the thermostable LOV domain from chloroflexus aggregans, *Crystals*, 2020, **10**(4), 256.

58 L. Wang, J. Gu, Y. Feng, M. Wang, Y. Tong, Y. Liu, X. Lyu and R. Yang, Enhancement of the isomerization activity and thermostability of cellobiose 2-epimerase from *Caldicellulosiruptor saccharolyticus* by exchange of a flexible loop, *J. Agric. Food Chem.*, 2021, **69**(6), 1907–1915.

59 R. Xing, H. Zhang, Q. Wang, Y. Hao, Y. Wang, J. Chen, X. Zhang and Z. Rao, Improved thermostability of maltooligosyl trehalose hydrolase by computer-aided rational design, *Syst. Microbiol. Biomanuf.*, 2025, **5**(1), 347–356.

60 S.-Y. Xu, R.-L. Chu, H.-T. Liu, C.-Y. Weng, Y.-J. Wang and Y.-G. Zheng, Computer-directed rational design enhanced the thermostability of carbonyl reductase LsCR for the synthesis of ticagrelor precursor, *Biotechnol. Bioeng.*, 2024, **121**(5), 1532–1542.

61 E. Zhu, X. Xiang, S. Wan, H. Miao, N. Han and Z. Huang, Discovery of the key mutation site influencing the thermostability of *Thermomyces lanuginosus* lipase by rosetta design programs, *Int. J. Mol. Sci.*, 2022, **23**(16), 8963.

62 Y. Li, L. Chen, X. Tang, W. Zhu, A. Ma, C. Shi and J. Li, Combined computer-aided predictors to improve the thermostability of nattokinase, *Foods*, 2023, **12**(16), 3045.

63 A. Dotsenko, J. Denisenko, D. Osipov, A. Rozhkova, I. Zorov and A. Sinitsyn, Testing and improving the performance of protein thermostability predictors for the engineering of cellulases, *J. Bioinf. Comput. Biol.*, 2023, **21**(2), 2330001.

64 S. Pan, S. Peng, C. Feng, H. Zhang, S. Qi, D. Lan and Y. Wang, Modifying loop regions in lipase from *Caldibacillus* thermoamylovorans for enhancing thermostability, *Int. J. Biol. Macromol.*, 2025, **309**, 142646.

65 R. Teng, J. Zhang, Z. Tu, Q. He and Y. Li, Computer-Aided design to improve the thermal stability of *Rhizomucor miehei* lipase, *Foods*, 2024, **13**(24), 4023.

66 Z. Qu, K. Chen, L. Zhang and Y. Sun, Computation-based design of salt bridges in petase for enhanced thermostability and performance for PET degradation, *ChemBioChem*, 2023, **24**(21), e202300373.

67 J. Stevensen, R. Z. Janatunaim, A. H. Ratnaputri, S. H. Aldafa, R. R. Rudjito, D. H. Saputro, S. Suhandono, R. M. Putri, R. Aditama and A. Fibriani, Thermostability and activity Improvements of PETase from *Ideonella sakaiensis*, *ACS Omega*, 2025, **10**(7), 6385–6395.

68 F. Liu, T. Wang, W. Yang, Y. Zhang, Y. Gong, X. Fan, G. Wang, Z. Lu and J. Wang, Current advances in the structural biology and molecular engineering of PETase, *Front. Bioeng. Biotechnol.*, 2023, **11**, 1263996.

69 A. Huang, Z. Chen, X. Wu, W. Yan, F. Lu and F. Liu, Improving the thermal stability and catalytic activity of ulvan lyase by the combination of FoldX and KnowVolution campaign, *Int. J. Biol. Macromol.*, 2024, **257**, 128577.

70 S. J. Costelloe, J. M. Ward and P. A. Dalby, Evolutionary analysis of the TPP-dependent enzyme family, *J. Mol. Evol.*, 2008, **66**(1), 36–49.

71 M. S. Hasson, A. Muscate, M. J. McLeish, L. S. Polovnikova, J. A. Gerlt, G. L. Kenyon, G. A. Petsko and D. Ringe, The crystal structure of benzoylformate decarboxylase at 1.6 Å resolution: diversity of catalytic residues in thiamin diphosphate-dependent enzymes, *Biochemistry*, 1998, **37**(28), 9918–9930.

72 E. S. Polovnikova, M. J. McLeish, E. A. Sergienko, J. T. Burgner, N. L. Anderson, A. K. Bera, F. Jordan, G. L. Kenyon and M. S. Hasson, Structural and kinetic analysis of catalysis by a thiamin diphosphate-dependent enzyme, benzoylformate decarboxylase, *Biochemistry*, 2003, **42**(7), 1820–1830.

73 H. Cui, H. Cao, H. Cai, K. E. Jaeger, M. D. Davari and U. Schwaneberg, Computer-assisted recombination (CompassR) teaches us how to recombine beneficial substitutions from directed evolution campaigns, *Chemistry*, 2020, **26**(3), 643–649.

74 A. Bornadel, C. O. Akerman, P. Adlercreutz, R. Hatti-Kaul and N. Borg, Kinetic modeling of lipase-catalyzed esterification reaction between oleic acid and trimethylolpropane: a simplified model for multi-substrate multi-product ping-pong mechanisms, *Biotechnol. Prog.*, 2013, **29**(6), 1422–1429.

75 F. Planas, M. J. McLeish and F. Himo, Computational study of enantioselective carboligation catalyzed by benzoylformate decarboxylase, *ACS Catal.*, 2019, **9**(6), 5657–5667.

76 D. Eisenberg, E. Schwarz, M. Komaromy and R. Wall, Analysis of membrane and surface protein sequences with the hydrophobic moment plot, *J. Mol. Biol.*, 1984, **179**(1), 125–142.

77 B. R. Caes, T. R. Van Oosbree, F. Lu, J. Ralph, C. T. Maravelias and R. T. Raines, Simulated moving bed chromatography: separation and recovery of sugars and ionic liquid from biomass hydrolysates, *ChemSusChem*, 2013, **6**(11), 2083–2089.

78 I. Arrieta, C. Gaudet, C. Haskell, S. Peacock, O. Tzschaetzsch and B.-C. Schulze, Industrial SMB chromatography as an alternative to the conventional refining of raw cane sugar, *Int. Sugar J.*, 2024, **149**(10), 669–677.